JOURNAL OF SOLID STATE CHEMISTRY 105, 528–534 (1993)

$Ca_{0.2}Na_{0.9}Fe_{2.9}O_5$: A New Me_4O_5 Structure Type

W. G. MUMME

Division of Mineral Products, CSIRO, Port Melbourne, Victoria 3207, Australia

Received August 12, 1992; accepted December 30, 1992

Examination of ferrite reactor product has resulted in the detection of a previously unreported Me_4O_5 oxide structure type with substituted composition $Ca_{0.11}Na_{1.11}(Fe_{2.84}Mg_{0.04})Si_{0.01}O_5$. Investigation of the system $Ca_xNa_{1-x}Fe_{3-x}O_5$, $x = 0.05$ to 0.3 has shown that the simplified composition of this phase is $Ca_{0.2}Na_{0.9}Fe_{2.9}O_5$ ($Z = 4$). Using the orthorhombic unit cell dimensions determined by indexing powder X-ray data, $a = 10.28$, 10.29(1), $b = 12.52$, 12.46(1), $c = 3.01$, 3.01(1) Å (for $Ca_{0.11}Na_{1.11}(Fe_{2.84}Mg_{0.04})Si_{0.01}O_5$ and $Ca_{0.2}Na_{0.9}Fe_{2.9}O_5$ respectively), and the most probable space group *Pnnm*, the crystal structure of this phase has been determined and refined from the powder data. $Ca_{0.2}Na_{0.9}Fe_{2.9}O_5$ may be described as having layers composed of Fe octahedra and tetrahedra on either side of (010) planes of Na trigonal prisms. The overall relationship to $CaFe_2O_4$, $CaFe_3O_5$, and the lillianite homologous series is discussed. The $Ca_{0.2}Na_{0.9}Fe_{2.9}O_5$ structure type is apparently stabilized by incorporation of the minor Ca into the $NaFe_3O_5$ composition.

Introduction

X-ray examination of the leached product of ferrites originally produced in a pilot plant constructed to investigate the feasibility of DARS (or the Direct Alkali Regeneration System) were carried out at CSIRO for the Associated Pulp and Paper Mills, Burnie, Tasmania. Along with the expected X-ray patterns, a set of unidentifiable reflections was seen to be present (*1*). DARS uses iron oxide as a causticizing agent to produce caustic from black liquor via beta-sodium ferrite, but impurities introduced with the iron oxide, for example, may cause additional phases to form in the system (*2*). It was decided that the observed set of X-ray lines represented such an impurity phase.

Some time later a more comprehensive set of the same X-ray peaks was observed in actual plant ferrite (*3*). SEM and EPMA studies of this sample (APPM specimen 25815) were subsequently carried out in order to identify the phase (*4*).

Chemical Composition and Unit Cell

The composition of the reactor phase, determined by EPMA and normalized to $\Sigma O = 20$, was $Ca_{0.43}Na_{4.43}(Fe_{11.37}Mg_{0.20})Si_{0.03}O_{20}$, one which very nearly balances charges. This overall composition was then mixed together from the appropriate predried, high purity chemicals ($CaCO_3$, Na oxalate, Fe_2O_3, MgO, and SiO_2) and subsequently reacted at 1050°C in a platinum crucible. Intermediate grindings of the product were carried out during a 20-hr heating time frame. The product was X-rayed and found to give a pattern which agreed with that of the unknown in 25815. Only very small peaks due to the presence of some beta sodium ferrite impurity were observed.

It was still not possible to identify the full X-ray pattern in the JCPDS powder X-ray data files; thus, in an attempt to further characterize this compound, the *d*-spacings were analyzed using the lattice indexing computer program constructed by Visser (*5*). In fact the powder X-ray data were com-

0022-4596/93 $5.00

TABLE I

X-RAY POWDER DATA FOR $Ca_{0.11}Na_{1.11}(Fe_{2.84}Mg_{0.04})Si_{0.01}O_5$ ($Z = 4$) AND $Ca_{0.2}Na_{0.9}Fe_{2.9}O_5$

	$Ca_{0.43}Na_{4.43}(Fe_{11.37}Mg_{0.20})Si_{0.03}O_{20}$			$Ca_{0.2}Na_{0.9}Fe_{2.9}O_5$	
I	d_{obs}	d_{calc}	hkl	d_{obs}	d_{calc}
20	6.270	6.261	020	6.220	6.228
10	5.153	5.142	200	5.138	5.143
5	4.765	4.756	210	4.757	4.757
25	3.977	3.974	220	3.964	3.966
5	3.307	3.306	310	3.304	3.306
5	3.241	3.241	230	3.230	3.231
5	3.129	3.131	040	3.115	3.114
10	2.927	2.926	011	2.922	2.922
100	2.673	2.674	240	2.664	2.664
35	2.571	2.571	400	2.572	2.571
80	2.543	2.543	211	2.539	2.541
30	2.441	2.441	031	2.434	2.435
5	2.400	2.399	221	2.395	2.396
5	2.375	2.378	420	2.370	2.377
		2.375	131		2.370
10	2.310	2.312	340	2.306	2.305
10	2.250	2.252	250	2.243	2.242
10	2.226	2.226	311	2.224	2.224
15	2.125	2.127	321	2.124	2.125
		2.123	141		2.117
20	1.925	1.925	051	1.919	1.918
10	1.866	1.866	421	1.865	1.865
5	1.833	1.833	341	1.830	1.829
30	1.770	1.770	431	1.769	1.768
5	1.586	1.586	370		
		1.585	630	1.586	1.585
10	1.566	1.565	080	1.561	1.557
20	1.541	1.541	451	1.539	1.538
5	1.522	1.521	171		
20	1.505	1.505	002	1.503	1.503
15	1.479	1.479	611	1.479	1.479
		1.479	112		
20	1.474	1.473	271	1.469	1.468
5	1.449	1.449	621		
		1.449	122		

pletely indexed with determined orthorhombic unit cell dimensions $a = 10.28(1)$, $b = 12.52(1)$, $c = 3.01(1)$ Å (Table I). Furthermore, the following systematic absences were suggested by this indexing; hkl, no conditions; $hk0$, no conditions; $0kl$, $k + l \neq 2n$; $h0l$, undetermined; $h00$, $h \neq 2n$; $0k0$, $k \neq 2n$; $00l$, $l \neq 2n$. These absences were interpreted to indicate *Pnam* and *Pnnm* as the two most likely space groups. Of these, the very plausible unit cell derived from the indexing program was noted to have its 3 Å axis better oriented in space group *Pnnm*, where atoms could lie at 0 or ½ levels along the short c-axis repeat. This is a condition which applies for many alkali or alkaline-earth ferrites; for example, $Na_xFe_xTi_{2-x}O_4$ (*6*). Volume relationships with $Na_xFe_xTi_{2-x}O_4$ also indicated that the stoichiometry of the new phase, based on the composition expressed above, should be expressed simply as Me_4O_5, with $Z = 4$.

Structure Solution

In the case that the unit cell and space group were correct it was considered that it should be possible to solve the structure of this compound by calculating a Patterson projection map using the 13 resolved $hk0$ X-ray powder data intensities (integrated intensities were measured using the powder diffractometer), and subsequently testing structure models by pattern refinement with the Rietveld method (*7*, *8*). Step-scanned powder X-ray data were collected with a Philips PW1710 diffractometer using monochromated Cu radiation over the range 5–100° 2θ, step size = 0.025°, step time = 10 sec, scatter slit = 1.0, divergence slit = 1.0°, receiving slit = 0.2°, and monochromator factor = 0.91. In the subsequent refinements a pseudo-Voigt profile shape function, corrected for asymmetry by the sum of four peaks method, was used. The counter zero, four polynomial background coefficients, peak halfwidths U, V, W (Gaussian), and K (Lorentzian), and the asymmetry parameter were the refined instrumental values. Un-ionized scattering coefficients were adopted for Ca, Na, Fe, and O.

The Patterson function $P(u, v)$ was calculated using SHELX76 (*9*), and the result is shown in Fig. 1. This Patterson projection is well resolved, with a set of peaks at the corners of the asymmetric unit, and others at ~¼, ⅛; ¼, ⅜; 0, ¼, and ½, ¼. The structure

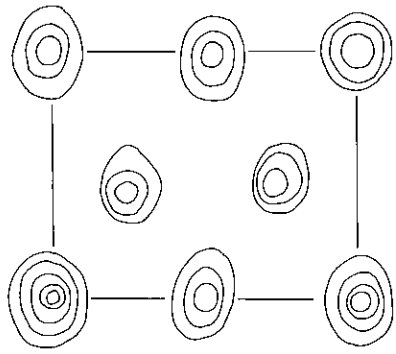

FIG. 1. Patterson function $P(u, v)$ projected onto (001), calculated using the resolved ($hk0$) intensity data from the powder X-ray data of $Ca_{0.43}Na_{4.43}(Fe_{11.37}Mg_{0.20})Si_{0.03}O_{20}$ (i.e., $Ca_{0.2}Na_{0.9}Fe_{2.9}O_5$-type). Vertical axis, $\frac{1}{2}a$; horizontal axis, $\frac{1}{2}b$.

solution was not immediately forthcoming but was reached after several models based on the Patterson projection were tested. When an atom was taken to occupy the origin position, the 2a (0, 0, 0; $\frac{1}{2}$, $\frac{1}{2}$, $\frac{1}{2}$) and 2d ($\frac{1}{2}$, 0, 0; 0, $\frac{1}{2}$, $\frac{1}{2}$) positions, together with the 4g positions ($\sim\frac{1}{4}$, $\sim\frac{1}{8}$, $\frac{1}{2}$; $\sim\frac{1}{4}$, $\sim\frac{3}{8}$, 0; and $\sim$0, $\sim\frac{1}{4}$, $\frac{1}{2}$) were progressively realized as the actual metal positions. However, this only became apparent through persistent refinement of the X-ray powder profile data using the Rietveld refinements, coupled with Fourier mapping. As the X-ray powder profile and the Bragg agreements were gradually improved with correct location of the metal atoms, the oxygen positions were deduced. Eventually, in this manner, the complete structure was determined, including the positions of the predominantly Na and Fe ordering. The final agreement factors were Bragg $R = 6.8$, $R_p = 18.1$, $R_{wp} = 24.7$, GOF = 2.1. The agreement profile is given in Fig. 2. Atom positions and simplified occupancies are given in Table IIa; bond lengths in Table IIIa.

X-Ray Study of Ca-Substituted $NaFe_3O_5$

After the above structure was determined and was proved to have Me_4O_5 stoichiometry it became apparent that, apart from the minor Ca and Mg, it could be approximately represented as $NaFe_3O_5$. This simple composition has never been reported in the Na_2O–Fe_2O_3 system, and although it seemed unlikely that it had been overlooked, it was prepared and reacted at $\sim$1050°C. The phase assemblage of Fe_2O_3 and $Na_3Fe_5O_9$, expected from several reported studies, was in fact confirmed at this composition.

X-ray studies were then carried out for the compositions $Ca_{2x}Na_{1-x}Fe_{3-x}O_5$ from $x = 0.05$ to $x = 0.3$, at the points $Ca_{0.1}Na_{0.95}Fe_{2.95}O_5$, $Ca_{0.2}Na_{0.9}Fe_{2.9}O_5$, $Ca_{0.4}Na_{0.8}Fe_{2.8}O_5$, and $Ca_{0.6}Na_{0.7}Fe_{2.7}O_5$. At $2x = 0.1$ the product was primarily the new phase discussed above, with small amounts of Fe_2O_3 and $Na_3Fe_5O_9$; at $2x = 0.2$ the product consisted only of the new phase (Table I), with $a = 10.29(1)$, $b = 12.46(1)$, $c = 3.01(1)$ Å. At $2x = 0.4$ and 0.6 increasing amounts of $CaFe_2O_4$ were observed, together with diminishing amounts of the new phase. Obviously this new "$NaFe_3O_5$" structure type forms only if stabilized by minor amounts of Ca.

TABLE II

ATOMIC COORDINATES AND TEMPERATURE FACTORS FOR (a) $Ca_{0.43}Na_{4.43}(Fe_{11.37}Mg_{0.20})Si_{0.03}O_{20}$ AND (b) $Ca_{0.2}Na_{0.9}Fe_{2.9}O_5$

Atom	Occupancy	x	y	z	B (Å^2)
	(a) $Ca_{0.43}Na_{4.43}(Fe_{11.37}Mg_{0.20})Si_{0.03}O_{20}$				
Fe1	Fe	.2201(7)	.1147(6)	½	1.34(25)
Fe2	Fe	.2399(9)	.3598(7)	0	3.53(33)
Fe3	Fe	.0000	.0000	0	1.53(37)
Fe4	Fe	.5000	.0000	0	1.62(33)
Na1	Na	−0.0198(18)	.2573(19)	½	2.88(49)
O1	O	.0987(26)	.1415(26)	0	2.26(79)
O2	O	.0619(29)	.3998(30)	0	3.77(81)
O3	O	.3343(25)	.0711(22)	0	1.27(56)
O4	O	.2677(28)	.2666(21)	½	2.00(68)
O5	O	.3832(25)	.4597(24)	0	1.16(54)
	(b) $Ca_{0.2}Na_{0.9}Fe_{2.9}O_5$				
Fe1	Fe	.2193(4)	.1156(3)	½	1.34(11)
Fe2	0.9 Fe + 0.1 Ca	.2386(5)	.3628(3)	0	1.71(13)[a]
Fe3	Fe	.0000	.0000	0	1.71(18)
Fe4	Fe	.5000	.0000	0	1.88(20)
Na1	0.9 Na + 0.1 Ca	−0.0233(10)	.2553(11)	½	3.97(27)
O1	O	.0893(14)	.1386(14)	0	2.26(41)
O2	O	.0702(16)	.4031(13)	0	3.77(41)
O3	O	.3308(15)	.0779(11)	0	1.27(38)
O4	O	.2706(16)	.2701(11)	½	2.00(38)
O5	O	.3748(14)	.4603(13)	0	1.16(35)

[a] B is 2.83 Å^2 if occupancy of Fe2 is 1.0 Fe.

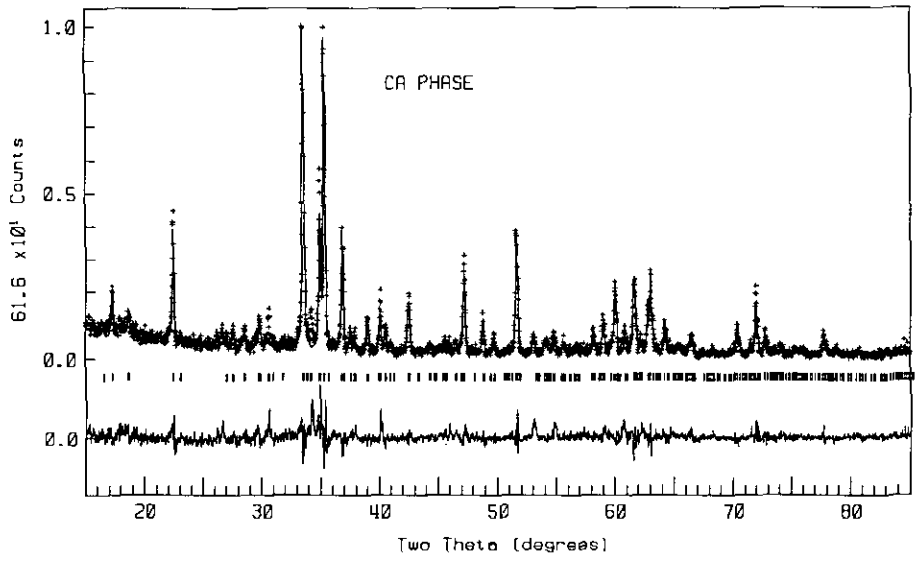

FIG. 2. Rietveld refinement results for $Ca_{0.43}Na_{4.43}(Fe_{11.37}Mg_{0.20})Si_{0.03}O_{20}$ (or $Ca_{0.2}Na_{0.9}Fe_{2.9}O_5$-type). Data points are given as crosses, calculated and difference profiles as solid lines. Reflection markers show the line positions.

Step-scanned X-ray data for the preparation synthesized at the composition $Ca_{0.2}Na_{0.9}Fe_{2.9}O_5$ were collected using the same set of conditions outlined above. The starting model used for the Rietveld refinement was the one in Table IIa. In this case, when refinement was concluded, the agreement parameters were Bragg R = 5.94, R_p = 16.1, R_{wp} = 20.4, GOF = 4.6. Tables IIb and IIIb give the atomic parameters and bond distances for $Ca_{0.2}Na_{0.9}Fe_{2.9}O_5$. It was considered that the most probable substitutions in this structure are the following: (1) 0.1 Ca + 0.9 Na occupy the trigonal prismatic Na site and (2) the balance of 0.1 Ca occupies one or some of the octahedral Fe sites. The results of refinements of this sort were again not conclusive. However, by introducing 0.1 Ca into Fe2, a higher than average B of 2.83 Å^2 reduced to 1.71 Å^2, more or less equivalent to the other Fe atoms; however, the B value for Na1, when it was substituted by 0.1 Ca, increased from 2.2 to 4.0 Å^2, (Table IIIb). Overall there was only a marginal decrease of the Bragg R value. This suggests the relatively unusual case of tetrahedral Ca; but it seems the full details of cation substitutions must wait for the results of a single crystal study.

TABLE III

BOND LENGTHS IN (a) $Ca_{0.43}Na_{4.43}(Fe_{11.37}Mg_{0.20})Si_{0.03}O_{20}$ AND (b) $Ca_{0.2}Na_{0.9}Fe_{2.9}O_5$

	(a) $Ca_{0.43}Na_{4.43}(Fe_{11.37}Mg_{0.30})Si_{0.03}O_{20}$	(b) $Ca_{0.2}Na_{0.9}Fe_{2.9}O_5$
Fe1–01	1.98 × 2	2.03 × 2
03	1.99 × 2	1.95 × 2
04	1.97	2.00
05	2.11	2.17
Fe2–02	1.90	1.81
04	1.93 × 2	1.93 × 2
05	1.93	1.86
Fe3–01	2.04 × 2	1.96 × 2
05	1.99 × 4	2.04 × 4
Fe4–03	1.92 × 2	2.00 × 2
02	2.06 × 4	2.06 × 4
Na1–01	2.42 × 2	2.39 × 2
02	2.48 × 2	2.57 × 2
04	2.67 × 2	2.62 × 2
04′	2.96	3.03
03	2.62	2.57
05	2.90	2.89

Note. Estimated standard deviations for bond distances are 0.06 Å.

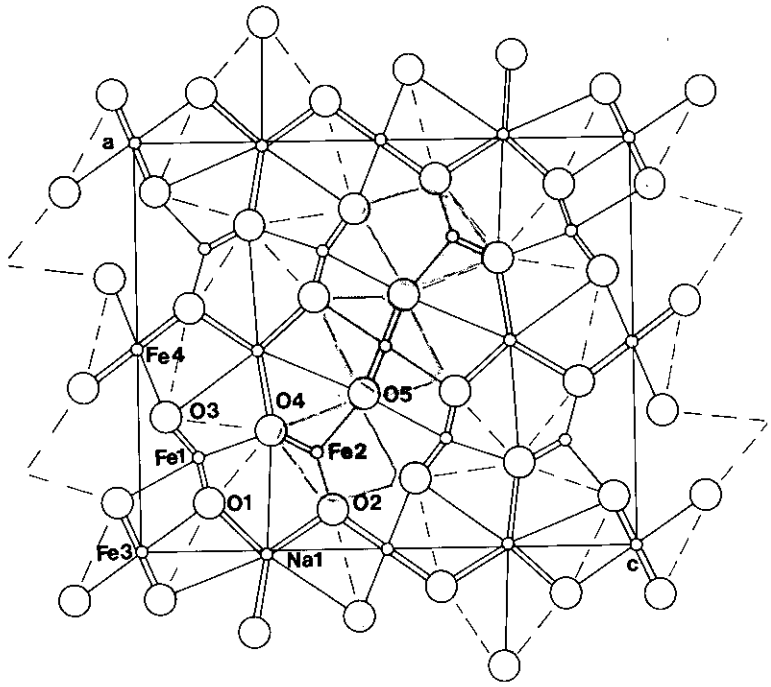

FIG. 3. Structure of $Ca_{0.2}Na_{0.9}Fe_{2.9}O_5$-type projected onto (001). Small labeled circles are metal atoms; large labeled circles are oxygen atoms. The octahedral/tetrahedral layers referred to in the text are outlined by dashed lines; one of the three-wide octahedral/tetrahedral chains is stippled.

The observed sum, Ca + Na > 1, in the reactor phase $Ca_{0.11}Na_{1.11}(Fe_{2.84}Mg_{0.04})Si_{0.01}O_5$ (Z = 4) in specimen 25815 is seen to be consistent with the suggested substitution mechanism for $Ca_{0.2}Na_{0.9}Fe_{2.9}O_5$, and therefore does not necessarily reflect analytical errors.

Description of the Structure

The crystal structure that was finally determined is illustrated in Fig. 3. It has five independent cation sites; three are octahedral, one is tetrahedral, and one is tricapped trigonal prismatic. The tricapped Na coordination prisms are aligned along planes (010) in the structure and are surrounded by the coordination octahedra of Fe1, Fe3, Fe4, and the tetrahedron of Fe2. In $Ca_{0.2}Na_{0.9}Fe_{2.9}O_5$ The Fe1–O distances range from 1.95 to 2.17 Å, mean = 2.02 Å; Fe3–O from 1.96 to 2.04 Å, mean = 2.01 Å; Fe4–O from 2.00 to 2.06 Å, mean = 2.04 Å. Fe2–O distances are from 1.81 to 1.93 Å, mean = 1.88 Å. Na1–O distances fall within the range 2.39 to 3.03 Å, mean = 2.63 Å.

Refinement of occupancy values in Na1 was not conclusive in proving that Ca substitutes for Na in this structure, although this appears to be the most probable location for half of the Ca. The average for the six Ca–O bonds to the triangular prism in $CaFe_2O_4$ (which is also tricapped) is a 2.42 Å (*10*). Similarly, the six prismatic Na–O bonds in the isolated tricapped trigonal prism in $Na_4Mn_4Ti_5O_{18}$ (*11*) have an average of 2.54 Å. In the structure of $Ca_{0.2}Na_{0.9}Fe_{2.9}O_5$ reported here the average of 2.53 Å determined for Na–O is not significantly shorter than this. However, the average bond distance of 1.92 Å for tetrahedral Fe2 is somewhat greater, for example, than the mean value 1.84 Å for the four independent Fe

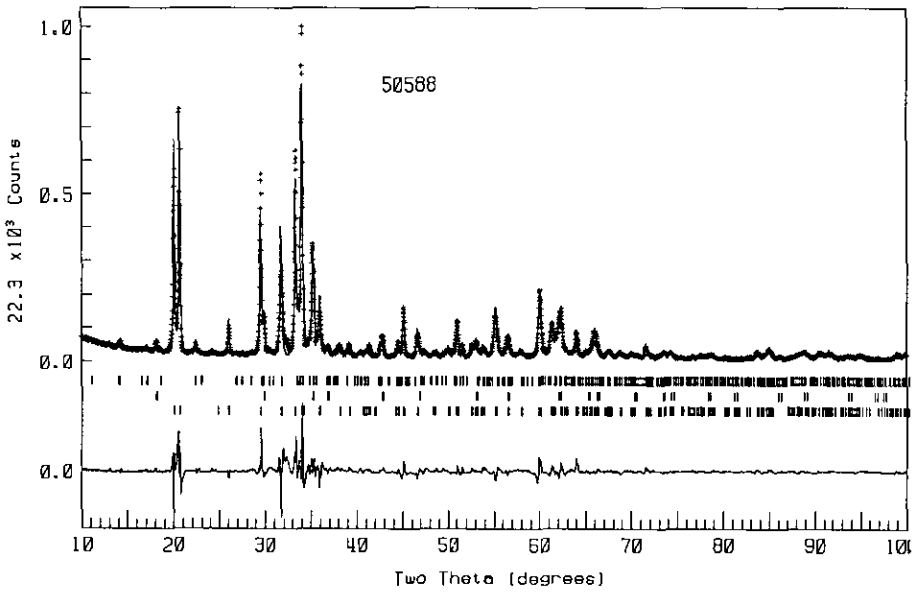

FIG. 4. Rietveld refinement results for the three-phase mixture of $Ca_{0.2}Na_{0.9}Fe_{2.9}O_5$-type and Na spinel-type in predominantly beta sodium ferrite. Reflection markers are in that order, from top to bottom.

tetrahedra found in the iron ore sinter product SFCA (*12*).

Discussion of the Structure

The crystal structure of $Ca_{0.2}Na_{0.9}Fe_{2.9}O_5$ is related to those of $CaTi_2O_4$ and $CaFe_2O_4$. $CaTi_2O_4$ represents the lillianite homolog ^{2,2}L, whereas $CaFe_2O_4$ is $^{\sim 2,2}$L; both structures have chains which are two octahedra wide in the layers lying between the sheets of Na trigonal prisms, but of the two, $CaFe_2O_4$ only approximates to a true lillianite homolog type (*13*). $Ca_{0.2}Na_{0.9}Fe_{2.9}O_5$ is in fact a $^{\sim 3,3}$L lillianite homolog member, with $CaFe_3O_5$ (*14*) representing the true ^{3,3}L structure. Lillianite, $Pb_3Bi_2S_6$, with four-wide chains of edge-shared octahedra in the intermediate layers, is the ^{4,4}L member after which the series is named (*15*).

Thus it turns out that, of the known ferrite structures, $CaFe_3O_5$ is most closely related to $Ca_{0.2}Na_{0.9}Fe_{2.9}O_5$. Because $CaFe_3O_5$ is *Cmcm*, the mirror planes produce in it a truly symmetrical ^{3,3}L lillianite homolog structure; on the other hand, in $Ca_{0.2}Na_{0.9}Fe_{2.9}O_5$ the chains of three Fe octahedra on one side of a Na trigonal prism degenerate into chains consisting of one Fe octahedron and two Fe tetrahedra on the other side (Fig. 2). Furthermore, the three-octahedra-wide chains in $Ca_{0.2}Na_{0.9}Fe_{2.9}O_5$ are not of pure lillianite type, because the central octahedron of the group, Fe4, is rotated by 180° from its usual orientation in the lillianite homologs. This is actually similar to the disposition of Fe octahedra observed in $CaFe_2O_4$.

Apparently the marginal size adjustments both in the Na trigonal prisms and in the Fe octahedral-cum-tetrahedral layers which result from the substitution of 0.2 Ca = 0.1 Na + 0.1 Fe are sufficient to allow this structure to form, whereas $NaFe_3O_5$ itself will not crystallize into this new, basic, and unique oxide structure type. Extending the relationship further to sulfide systems, the structure might possibly be represented by

the composition $Cu^{2+}PbBi_2S_5$, with tetrahedral Cu, trigonal prismatic and octahedral Pb, and octahedral Bi.

Quantitative Ferrite Phase Analysis

Other specimens of reactor beta sodium ferrite product sometimes include a spinel-like sodium iron oxide (*16*) as well as the above described $Ca_{0.2}Na_{0.9}Fe_{2.9}O_5$-type phase as impurities. Figure 4 shows the calculated and observed X-ray profiles for a typical product of this sort after refinement of the X-ray data by the Rietveld method, with all three phases included in the refinement calculations. Using the relationship between the individual Rietveld scale factors derived for each phase and their ZMV values it is possible to calculate the relative phase abundances in the ferrite (*17*). In the case illustrated in Fig. 4, it is estimated that this ferrite contains 7.6 wt% of $Ca_{0.2}Na_{0.9}Fe_{2.9}O_5$-type, 17.5 wt% of the Na-spinel type, and 74.9 wt% of beta ferrite (total normalized to 100 wt%). The usefulness of this approach is that, from such phase abundance estimates, it should be possible to calculate the plant leaching efficiencies and caustic reclamation values which might be achieved for current plant product.

References

1. W. G. MUMME, CSIRO Report (restricted) MPC/M-001 (1987).
2. C. NAGAI, S. MATSUMOTO, AND H. HATTORI, *Pulp Paper Can.* **92,** 35 (1991).
3. W. G. MUMME AND N. V. Y. SCARLETT, CSIRO Report (restricted) MPC/M-116 (1989).
4. N. V. Y. SCARLETT AND W. G. MUMME, CSIRO Report (restricted) MPC/M-229 (1990).
5. J. W. VISSER, *J. Appl. Crystallogr.* **2,** 89 (1969).
6. W. G. MUMME AND A. F. REID, *Acta Crystallogr. Sect. B* **24,** 625 (1968).
7. H. M. RIETVELD, *Acta Crystallogr.* **22,** 151 (1967).
8. R. J. HILL AND C. J. HOWARD, Aust. Atomic Energy Commission Report No. M112, Lucas Heights Res. Labs, NSW, Australia.
9. G. M. SHELDRICK, "SHELX76" (1976).
10. B. F. DECKER AND J. S. KASPER, *Acta Crystallogr.* **10,** 332 (1957).
11. W. G. MUMME, *Acta Crystallogr. Sect. B* **24,** 1114 (1968).
12. J. D. G. HAMILTON, B. F. HOSKINS, W. G. MUMME, W. E. BORBIDGE, AND M. A. MONTAGUE, *Neues Jahrb. Mineral. Abh.* **161,** 1 (1989).
13. E. MAKOVICKY, *Neues Jahrb. Mineral. Abh.* **131,** 187 (1977).
14. O. EVRARD, B. MALAMAN, F. JEANOT, A. COURTOIS, H. ALEBOUYEH AND R. GERADIN, *J. Solid State Chem.* **35,** 112 (1980).
15. E. MAKOVICKY, *Neues Jahrb. Mineral. Abh.* **130,** 264 (1977).
16. J. THERY AND R. COLLONGUES, *C. R. Hebd. Seances Acad. Sci.* **250,** 1070 (1960).
17. R. J. HILL AND C. J. HOWARD, *J. Appl. Crystallogr.* **20,** 467 (1987).